

Giant multicaloric response of bulk Fe₄₉Rh₅₁

Enric Stern-Taulats,¹ Teresa Castán,¹ Antoni Planes,¹ Laura H. Lewis,² Radhika Barua,³ Sabyasachi Pramanick,⁴ Subham Majumdar,⁴ and Lluís Mañosa¹

¹*Departament de Física de la Matèria Condensada, Facultat de Física, Universitat de Barcelona, Martí i Franquès 1, E-08028 Barcelona, Catalonia*

²*Department of Chemical Engineering and Department of Mechanical Engineering, Northeastern University, Boston, Massachusetts 02115, USA*

³*Department of Chemical Engineering, Northeastern University, Boston, Massachusetts 02115, USA*

⁴*Department of Solid State Physics, Indian Association for the Cultivation of Science, Jadavpur, Kolkata 700 032, India*

(Received 19 October 2016; revised manuscript received 28 February 2017; published 17 March 2017)

We report on the multicaloric response of the Fe₄₉Rh₅₁ alloy under the combined application of hydrostatic pressure and magnetic field. Experimental data are complemented by a mean field model that takes into account the interplay between structural and magnetic degrees of freedom. A large multicaloric strength has been found for this alloy, and it is shown that a suitable combination of pressure and magnetic field enables the sign of the entropy change to be reversed and thus the multicaloric effect can be tuned from conventional to inverse. It is also shown that an extended temperature window for the multicaloric effect can be achieved by taking advantage of the coupling between structure and magnetism which enables a cross response of the alloy under the application of different external fields. Mean field calculations remarkably reproduce experimental results.

DOI: [10.1103/PhysRevB.95.104424](https://doi.org/10.1103/PhysRevB.95.104424)

I. INTRODUCTION

Interest in the study of materials with giant caloric effects has experienced an enormous increase in the last decade owing to the fact that this category of materials features excellent candidates for the development of solid-state cooling devices. They can replace or augment current refrigerators and cooling systems which are based on the compression and expansion of environmentally harmful fluids. Realization of these systems will result in a more efficient and environmentally friendly cooling technology.

Significant caloric effects typically occur in materials undergoing a ferroic phase transition [1–3], and particularly large (giant) effects are observed when the ferroic transition is first order in nature. In this scenario the latent heat that accompanies the first-order transition gives rise to large temperature or entropy changes, induced by the application and removal of the external field thermodynamically conjugated to the ferroic property under adiabatic or isothermal conditions. At present, a variety of materials have been reported to exhibit giant caloric effects, which are classified by the nature of the applied field (and hence by the ferroic property) as magnetocaloric [4], electrocaloric [5], and mechanocaloric [6] (which includes elastocaloric and barocaloric) effects, for magnetic, electric, and mechanical (uniaxial stress and hydrostatic pressure) fields, respectively.

Many giant caloric materials exhibit strong coupling between different degrees of freedom and therefore the ferroic transition involves the spontaneous development of more than one ferroic property. Hence, changes in magnetization and in electric polarization at the phase transition are typically accompanied by structural changes (with an associated lattice strain), allowing the ferroic transition to be induced by the application of more than one external field. This cross response implies that changes in magnetization (or in polarization) can be induced by mechanical fields while structural changes can also be induced by magnetic (or electric) fields thus giving rise

to a multiferroic behavior. From the point of view of caloric effects, the simultaneous or sequential application of more than one external field can give rise to multicaloric effects [3].

While single caloric effects have received a great deal of attention and advancement to date [7], until now little research effort has been devoted to the study of multicaloric effects, despite the belief that these effects can improve caloric performance and overcome some drawbacks such as irreversibilities due to hysteresis, limited operational range, etc. Although theoretical frameworks to study multicaloric effects have been developed with sufficient detail [8–11], at present there is only a very limited number of experimental studies on such systems [12–17], these experimental reports typically focus on the effect of hydrostatic pressure on the magnetocaloric effect. In the present work, we combine experiments and modeling to obtain a complete description of the multicaloric response of a representative model material Fe₄₉Rh₅₁. We provide quantitative data of the entropy change associated with the combined effect of pressure and magnetic field. It is shown that the temperature range and magnitude of the resultant entropy changes of this system may be tailored to defined values through coordinated application of pressure and magnetic field.

FeRh has received considerable attention in recent years [18–22], and it is a representative material ideal to investigate the fundamentals of multicaloric effects. This compound crystallizes in the CsCl cubic structure and, for compositions close to the stoichiometric composition Fe₅₀Rh₅₀, it undergoes a magnetostructural transition from a low-temperature antiferromagnetic (AFM) phase to a high-temperature ferromagnetic (FM) phase. In the FM state, Fe atoms have a $\sim 3 \mu_B$ moment and Rh atoms $\sim 1 \mu_B$, while in the AFM state there is no appreciable magnetic moment on the Rh atoms and the Fe atoms have $\sim 3 \mu_B$ moment with opposite sign on successive layers of (111) iron planes [23]. At the phase transition there is no change in the crystal symmetry but the lattice

isotropically expands and the volume of the FM unit cell is $\sim 1\%$ larger than that of the AFM phase. Giant magnetocaloric [24], elastocaloric [25], and barocaloric [26] effects have been reported for this compound. Moreover, magnetocaloric and barocaloric strengths of FeRh have been found to be among the highest reported values for magnetocaloric and barocaloric materials, and both effects exhibit a good reproducibility upon magnetic field and pressure cycling [27,28].

This paper is organized as follows: Experimental details are given in Sec. II. Useful thermodynamic considerations are provided in Sec. III, and they are expanded in Appendix A. A mean field model is presented in Sec. IV, and a more detailed description of it is given in Appendix B. Results are presented and discussed in Secs. V–VIII where both data from experiments and from the model are presented in a comparative way. Finally, we provide a brief summary of our work in Sec. IX.

II. EXPERIMENTAL DETAILS

A polycrystalline sample of nominal composition $\text{Fe}_{49}\text{Rh}_{51}$ was prepared by arc melting. Details on sample preparation and heat treatment are given in Ref. [26]. From the prepared button, a sample with the shape of a needle (28.9 mg) was cut using a diamond saw. Magnetization measurements at hydrostatic pressure (from ambient up to 5.1 kbar) were performed using a superconducting quantum interference device (Quantum Design, SQUID) magnetometer in magnetic fields up to 5 T and in the temperature range $220 < T < 390$ K. Hydrostatic pressure was applied to the sample using a CuBe piston clamp pressure cell (Mcell 10 manufactured by Almax EasyLab). To minimize errors due to differential thermal contraction between the metallic components of the pressure cell and the pressure transmitting medium, the temperature sweep rate during measurement was set at 1 K/min. The pressure inside the cell was calibrated *in situ* by measurement of the shift of the superconducting transition temperature of a Sn standard.

III. THERMODYNAMIC CONSIDERATIONS

The multicaloric effect refers to the isothermal entropy change (or adiabatic temperature change) resulting from the combined application of two external fields. From a thermodynamic point of view in equilibrium there is no distinction on whether the two fields are applied simultaneously or sequentially.

In the particular case of magnetic field and hydrostatic pressure as the external stimuli, the resulting multicaloric entropy change is

$$\begin{aligned} \Delta S(T, 0 \rightarrow H, 0 \rightarrow p) \\ = \Delta S(T, 0, 0 \rightarrow p) + \Delta S(T, 0 \rightarrow H, p), \end{aligned} \quad (1)$$

where for simplicity we take atmospheric pressure as our zero pressure state.

It is worth noting that while the first term in Eq. (1) represents the standard barocaloric effect (in the absence of magnetic field), the second term differs from the standard magnetocaloric effect (which is computed from magnetization data measured at atmospheric pressure). It is given by (see

Appendix A)

$$\begin{aligned} \Delta S(T, 0 \rightarrow H, p) \\ = \Delta S(T, 0 \rightarrow H, 0) + \int_0^p \int_0^H \frac{\partial}{\partial T} \left(\frac{\partial M}{\partial p} \right)_{T, H} dp dH, \end{aligned} \quad (2)$$

where $\Delta S(T, 0 \rightarrow H, 0)$ quantifies the standard magnetocaloric effect, and the second term is a consequence of the interplay between magnetic and structural degrees of freedom. Only in the absence of interplay $\Delta S(T, 0 \rightarrow H, 0 \rightarrow p)$ is the sum of the standard magnetocaloric and standard barocaloric effects.

In principle, computation of the barocaloric entropy change would require data on the pressure and temperature dependencies of the specific volume. However, it can also be computed from magnetization data as a function of temperature, pressure, and magnetic field. Therefore the total multicaloric entropy change can be computed (indirect method) from the knowledge of $M(T, H, p)$ as follows (see Appendix A):

$$\begin{aligned} \Delta S(T, 0 \rightarrow H, 0 \rightarrow p) \\ = \int_0^p \left(\frac{\partial M}{\partial H} \right)_{T, p} \left(\frac{\partial M}{\partial T} \right)_{p, H} dp + \int_0^H \left(\frac{\partial M}{\partial T} \right)_{p, H} dH \\ + \int_0^p \int_0^H \frac{\partial}{\partial T} \left(\frac{\partial M}{\partial p} \right)_{T, H} dp dH, \end{aligned} \quad (3)$$

where for convenience we have used expression (A16) for the standard barocaloric effect.

It must be mentioned that Eqs. (1)–(3) demonstrate that knowledge of the standard magnetocaloric and barocaloric effects in a given material are not sufficient to determine its multicaloric behavior, and information on the cross response of the material to the fields that are nonconjugated to the order parameter are required (either the volume dependence on magnetic field or the magnetization dependence on pressure).

IV. MEAN FIELD MODELING

In order to interpret the experimental behavior and to gain better insight into the FeRh multicaloric response, we have developed a mean field model for the free energy of the system that describes the AFM-FM phase transition. The model includes a magnetovolumic coupling term to account for the unit cell volume change at the transition. This coupling term is restricted to the minimum order allowed by symmetry and the effect of external fields such as hydrostatic pressure p and magnetic field H are included. The procedure, explained in detail in Appendix B, renders the following variational Gibbs energy function per magnetic atom:

$$\begin{aligned} g^* = \frac{g}{z J_{\text{FeRh}}^{(1)}} = & -\frac{1}{2} m_{\text{Fe}} m_{\text{Rh}} - \frac{J^*}{4} (m_{\text{Fe}}^2 - \eta_{\text{Fe}}^2) \\ & + \frac{T^*}{8} [(1 + m_{\text{Fe}} + \eta_{\text{Fe}}) \ln(1 + m_{\text{Fe}} + \eta_{\text{Fe}}) \\ & + (1 - m_{\text{Fe}} - \eta_{\text{Fe}}) \ln(1 - m_{\text{Fe}} - \eta_{\text{Fe}}) \\ & + (1 + m_{\text{Fe}} - \eta_{\text{Fe}}) \ln(1 + m_{\text{Fe}} - \eta_{\text{Fe}}) \end{aligned}$$

$$\begin{aligned}
& + (1 - m_{\text{Fe}} + \eta_{\text{Fe}}) \ln(1 - m_{\text{Fe}} + \eta_{\text{Fe}}) \\
& + 2(1 + m_{\text{Rh}}) \ln(1 + m_{\text{Rh}}) + 2(1 - m_{\text{Rh}}) \ln(1 - m_{\text{Rh}}) \\
& - 8 \ln 2] + \frac{1}{2} \alpha_0^* \omega^2 - \alpha_1^* \omega (m_{\text{Fe}} + m_{\text{Rh}})^2 - \alpha_2^* \omega \eta_{\text{Fe}}^2 \\
& - H^* (m_{\text{Fe}} + m_{\text{Rh}}) + P \Omega_0^* \omega, \quad (4)
\end{aligned}$$

where m_{Fe} and m_{Rh} are the order parameters that describe the ferromagnetism of the sublattices of Fe and Rh, and η_{Fe} is the antiferromagnetic order parameter of Fe; ω is the relative volume change (with respect to a reference volume Ω_0); α_1 and α_2 are magnetostriction coefficients, and α_0 is the inverse of the compressibility. J is an effective exchange interaction parameter and z refers to the coordination number for first neighbors. The thermodynamic Gibbs free energy is then obtained by replacing the order parameters by those that minimize the above variational function.

The model can be used to study multicaloric effects in FeRh. Indeed, the entropy S of the system can be directly computed from Eq. (4) by employing the thermodynamic definition of S ,

$$\begin{aligned}
S(M_{\text{Fe}}, m_{\text{Rh}}, \eta_{\text{Fe}}) &= - \left[\frac{\partial g^*}{\partial T^*} \right]_{P, H} \\
&= S_{\text{Fe}}(m_{\text{Fe}}, \eta_{\text{Fe}}) + S_{\text{Rh}}(m_{\text{Rh}}), \quad (5)
\end{aligned}$$

where $m_{\text{Fe}}(T, H, p)$, $m_{\text{Rh}}(T, H, p)$, and $\eta_{\text{Fe}}(T, H, p)$ are the equilibrium order parameters obtained after minimization of the variational free energy function (4). The isothermal entropy change for the multicaloric effect can be calculated from

$$\begin{aligned}
\Delta S_T(T, 0 \rightarrow H, 0 \rightarrow p) \\
= S(T, H, p) - S(T, H = 0, p = 0). \quad (6)
\end{aligned}$$

The experimental data used to fit the model parameters are the relative volume change at the magnetostructural transition [29], the transition temperatures at atmospheric pressure [30], and at the pressure where the FM phase disappears [31,32]. With only these experimental input data, the model is able to reproduce the phase transformation features of the FeRh CsCl-type compound and its multicaloric behavior.

From the model it is possible to compute the phase diagram in an extended range of parameters. Figure 1 shows the theoretical results (dashed lines) for the phase diagram of Fe₅₀Rh₅₀ and Fe₄₉Rh₅₁ as a function of the pressure (a) and the magnetic field (b), compared with available experimental data [26,30–32]. It is apparent that the model nicely reproduces the experimental data of the FeRh system over a broad range of p , H , and T .

V. MAGNETIZATION AS A FUNCTION OF PRESSURE AND MAGNETIC FIELD

Figure 2 shows illustrative examples of the magnetization curves recorded during cooling and heating the sample at selected (constant) values of applied magnetic field H and hydrostatic pressure p . On cooling, the sample undergoes the forward transition from a saturated FM state to an AFM state; the reverse transition takes place on heating with a thermal hysteresis of ~ 10 K. The inflection point of the M vs T curves is taken as the characteristic transition temperature T_i . A small increase in the magnetization of both FM and AFM phases with

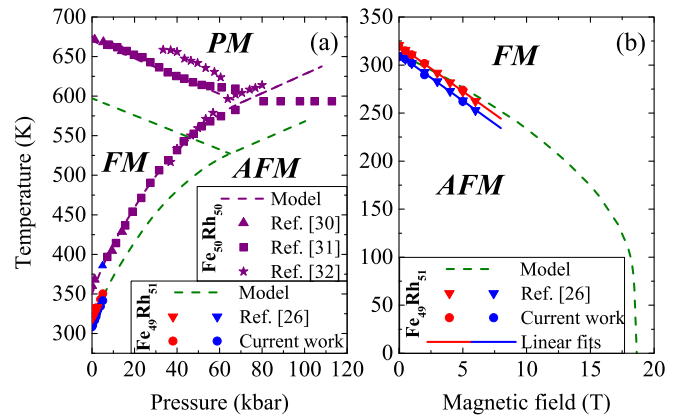


FIG. 1. Phase diagram of FeRh. Transition temperature as a function of pressure p (a) and magnetic field H (b) for Fe₅₀Rh₅₀ and Fe₄₉Rh₅₁. Results from the mean field model are denoted by dashed lines while symbols correspond to experimental data.

increasing magnetic field is measured, which results in a small increase in the magnetization change (ΔM_i) at the FM-AFM phase transition. On the other hand, ΔM_i slightly decreases with increasing pressure ($\sim 2\%$ decrease for $p = 5$ kbar). The FM-AFM transition shifts to lower temperatures with increasing magnetic field H while it moves to higher T with increasing applied pressure p . This behavior is consistent with the scenario that H stabilizes the high-magnetization FM phase, while p stabilizes the low-volume AFM phase. The measured pressure dependence of T_i , determined in the absence of magnetic field [$T_i(p, H = 0)$], and the measured magnetic field dependence at atmospheric pressure [$T_i(p = 0, H)$] are in perfect agreement with previous reports [26,27] (for simplicity atmospheric pressure is referred here as $p = 0$).

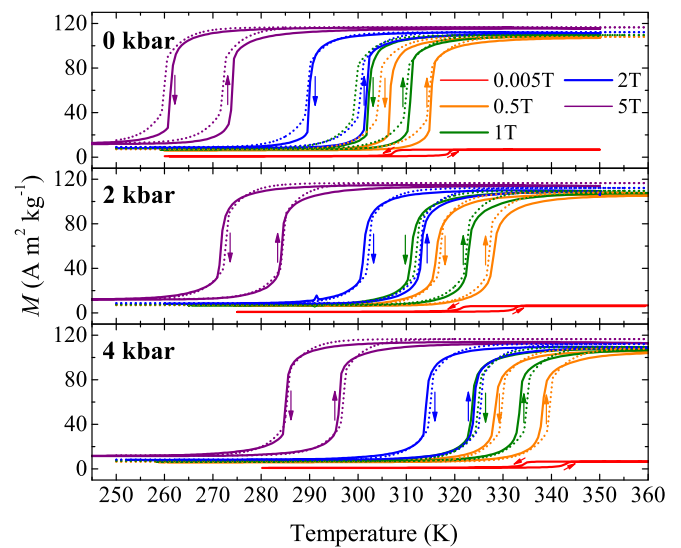


FIG. 2. Examples of magnetization curves as a function of temperature at selected values of magnetic field H and hydrostatic pressure p . Solid lines correspond to experimental data and dotted lines correspond to the fitted curves. The arrows indicate cooling and heating runs.

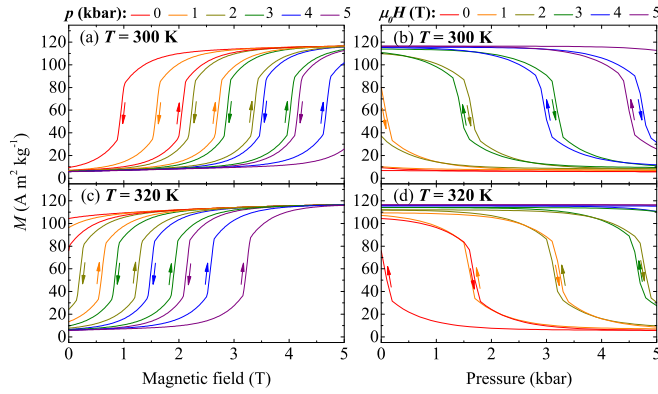


FIG. 3. Isothermal magnetization as a function of applied magnetic field of $\text{Fe}_{49}\text{Rh}_{51}$ at selected values of pressure p , at 300 K (a) and at 320 K (c). Isothermal magnetization as a function of pressure at selected values of magnetic field H , at 300 K (b) and 320 K (d).

Since experimental magnetization values are only known for given values of magnetic field and hydrostatic pressure, for numerical analysis of caloric and multicaloric effects it is convenient to fit an analytical function $M(T, H, p)$ to obtain magnetization over the entire (T, H, p) thermodynamic phase space. We assume that the transition extends in temperature from $T_t - \delta T$ up to $T_t + \delta T$ (where T_t is the transition temperature and the best fit is obtained for $\delta T = 0.6$ K). The experimental data have been fitted as follows:

(i) An hyperbolic tangent function has been used for temperatures T within the transition region $T_t - \delta T \leq T \leq T_t + \delta T$:

$$M = \frac{1}{2} [M_{\text{AFM}} + M_{\text{FM}}] + \frac{1}{2} \left[(M_{\text{AFM}} - M_{\text{FM}}) \tanh \left(\frac{T - T_t}{W} \right) \right], \quad (7)$$

where M_{AFM} and M_{FM} are, respectively, the magnetization of the AFM and FM phases, and W is a parameter that accounts for the temperature spread of the transition.

(ii) Beyond the transition region, an exponential function has been used to describe the temperature dependence of the magnetization in both the AFM and FM phases, as follows:

$$M = M_{\text{AFM}} + [M(T_t - \delta T) - M_{\text{AFM}}] \times \exp[k_1(T - T_t + \delta T)], \quad T < T_t - \delta T, \quad (8)$$

$$M = M_{\text{FM}} + [M(T_t + \delta T) - M_{\text{FM}}] \times \exp[k_2(T_t - T + \delta T)], \quad T > T_t + \delta T, \quad (9)$$

where k_1 and k_2 are positive constants.

Examples for the comparison between the fitted curves and the experimental data are shown in Fig. 2.

Figure 3 shows examples of the magnetic field dependence of the isothermal magnetization [Figs. 3(a) and 3(c)] at selected values of hydrostatic pressure, and of the pressure dependence of the isothermal magnetization [Figs. 3(b) and 3(d)], at selected values of magnetic field. Figure 4 shows the combined dependence of the isothermal magnetization upon hydrostatic pressure and magnetic field, for selected values of temperature.

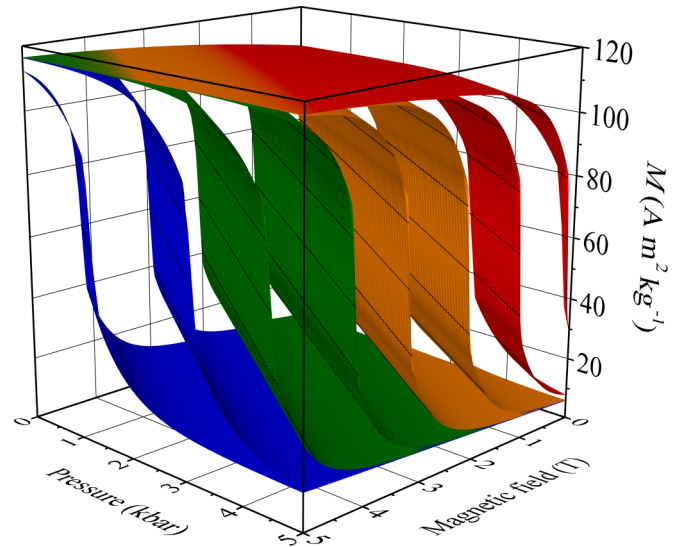


FIG. 4. Isothermal magnetization as a function of magnetic field and pressure for $\text{Fe}_{49}\text{Rh}_{51}$. Data correspond to 340 K (red), 320 K (orange), 300 K (green), and 280 K (blue). For each temperature the surfaces on the left side of the figure correspond to application of field and removal of pressure (AFM to FM transition), while the surfaces on the right correspond to removal of field and application of pressure (FM to AFM transition).

VI. THERMODYNAMIC PHASE DIAGRAM

Figure 5(a) shows the thermodynamic phase diagram for $\text{Fe}_{49}\text{Rh}_{51}$ where experimental data are indicated by solid symbols. The linear pressure and magnetic field dependence of T_t results in planar surfaces that separate AFM and FM regions, while the region between the planes represents the two-phase hysteretic region. The combined p and H dependence of the transition temperature is quantified as $T_t(H, p) = 309.3 - 9.9\mu_o H + 6.3p$ for the FM to AFM transition and

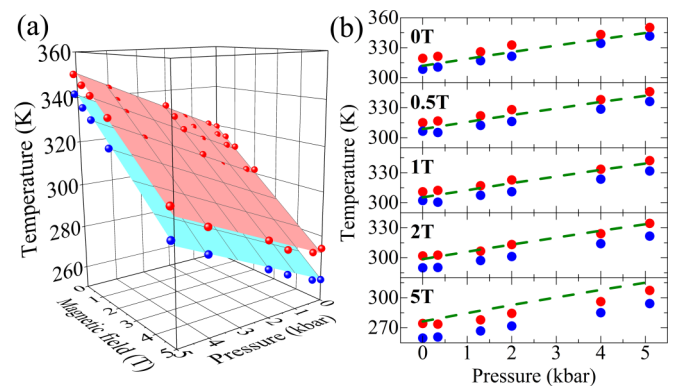


FIG. 5. (a) Transition temperature as a function of magnetic field and pressure for $\text{Fe}_{49}\text{Rh}_{51}$. Upper red plane corresponds to the AFM to FM transition, and lower blue plane to the FM to AFM transition. Solid symbols stand for experimentally measured values. (b) Transition temperature as a function of pressure for selected values of magnetic field. Red symbols stand for experimental data for the AFM to FM transition, and blue symbols stand for experimental data for the FM to AFM transition. Dashed lines correspond to data derived from the mean field model.

$T_t(H, p) = 319.5 - 9.5\mu_0 H + 6.2p$ for the AFM to FM transition. Figure 5(b) compares the pressure dependence (at fixed magnetic field) of the transition temperature obtained from experiments with that derived from the mean field model (dashed lines). In spite of the fact that the model does not explicitly account for thermal hysteresis, good agreement exists between the two sets of data for fields up to 2 T. For larger fields, the model slightly overestimates transition temperatures. For this reason, in the following discussion we will restrict our study to the system response for $\mu_0 H \leq 2$ T.

VII. HYSTERESIS

As expected for a first-order transition, the magnetostructural transition in Fe₄₉Rh₅₁ takes place with hysteresis. When the transition is driven by temperature, hysteresis amounts ~ 10 K (see Fig. 2), when it is driven by magnetic field, it amounts to ~ 1.1 T, and in the case of hydrostatic pressure, it is ~ 1.7 kbar (see Fig. 3). It is worth noticing that by taking into account the obtained values of dT_t/dH and dT_t/dp both, the hysteresis in magnetic field and in pressure correspond to a thermal hysteresis of ~ 10 K. This is consistent with the fact that AFM and FM phases in our sample are separated by plane surfaces in the thermodynamic phase diagram [Fig. 5(a)] which ensures that the hysteresis magnitude is constant, and the values given above are independent of T , H , and p .

It has recently been reported that in a metamagnetic Heusler shape memory alloy, magnetization of the sample at atmospheric pressure and demagnetization under an applied hydrostatic pressure of 1.3 kbar resulted in a significant reduction of hysteresis [16]. This phenomenon is attributed to the shift of the first-order transition to lower temperatures with magnetic field, and the shift towards higher temperatures with hydrostatic pressure. In our Fe₄₉Rh₅₁ specimen magnetic field and pressure also shift the magnetostructural transition in a similar way, as discussed in previous sections and therefore a reduction of hysteresis is also expected from the combined effect of H and p . This phenomenon is illustrated in Fig. 6(a) which shows isothermal magnetization loops at atmospheric pressure and under an applied pressure of 1.7 kbar. It is seen that the hysteresis is almost suppressed by magnetizing the sample at atmospheric pressure and demagnetizing it under 1.7 kbar. However, such a reduction in hysteresis is only apparent because the reduction in magnetic field occurs at the expense of hysteresis in pressure. This fact is illustrated in Fig. 6(b) which indicates the actual thermodynamic path followed by the sample in such a combined magnetic field/pressure cycle.

It is instructive to compare the energy dissipated in a magnetic field loop (at atmospheric pressure) E_H , to that dissipated in the combined cycle $E_{H,p}$. These quantities are computed as

$$E_H = \mu_0 \oint H dM(T, H, 0) \quad (10)$$

and

$$E_{H,p} = E^I + E^{II} + E^{III} + E^{IV}, \quad (11)$$

where E^I , E^{II} , E^{III} , and E^{IV} correspond, respectively, to the work associated with trajectories I, II, III, and IV indicated in

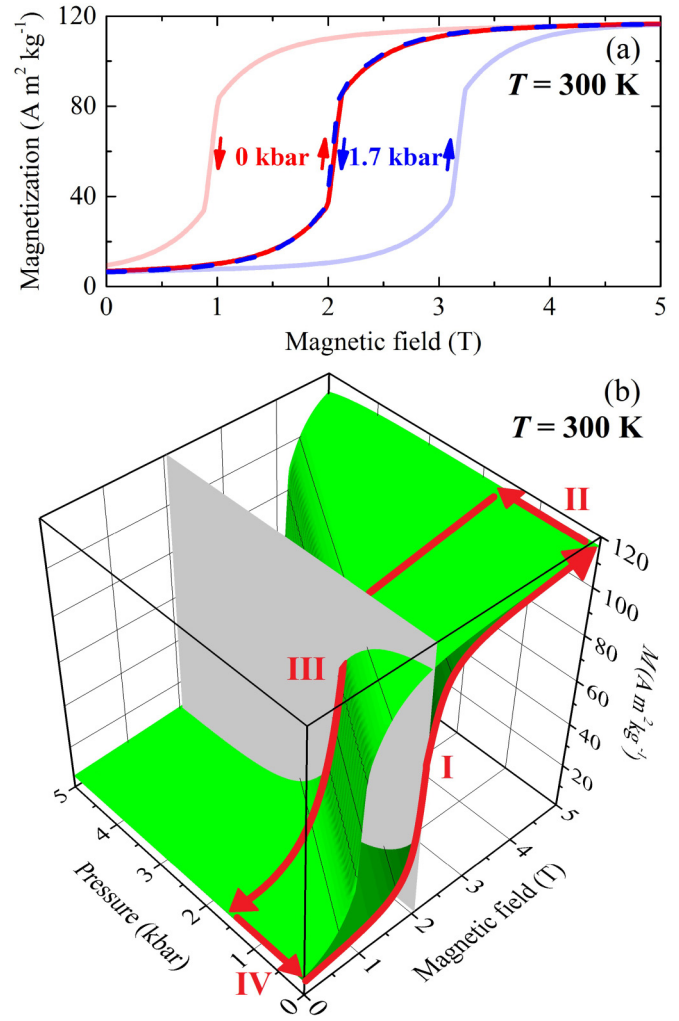


FIG. 6. (a) Isothermal magnetization obtained on increasing and decreasing magnetic field at selected (constant) values of hydrostatic pressure. (b) Isothermal magnetization surface as a function of pressure and of magnetic field. The red arrows indicate a complete loop corresponding to an increase of magnetic field at atmospheric pressure (path I), application of a 1.7 kbar pressure in the FM phase (path II), removal of the magnetic field under 1.7 kbar (path III), and removal of hydrostatic pressure in the AFM phase (path IV).

Fig. 6. Under the assumption that volume compressibilities of AFM and FM phases are similar ($\kappa_{AFM} \simeq \kappa_{FM}$), and

$$\int_I H dM(T, H, 0) \simeq \int_{III} H dM(T, H, p), \quad (12)$$

the energy dissipated in the multicaloric cycle is given by

$$E_{H,p} \simeq \Delta p \Delta v, \quad (13)$$

where Δv is the difference in the atomic volume of the two phases.

For our Fe₄₉Rh₅₁ sample we obtain $E_H \simeq 115$ J kg⁻¹ and $E_{H,p} \simeq 170$ J kg⁻¹. While the energy corresponding to the multicaloric loop is marginally larger than that corresponding to the magnetic field loop (at constant pressure), it is worth noticing that both quantities are much smaller than the latent heat of the transition (~ 3300 J kg⁻¹). With regards to cooling

applications, it must be taken into account that a reduced hysteresis enhances the reproducibility of the caloric effects [33,34], and under certain circumstances it can result very beneficial to apply both external stimuli even if the energy dissipated in the multicaloric cycle is slightly larger than that corresponding to a pure magnetic field cycle.

VIII. CALORIC AND MULTICALORIC ENTROPY CHANGES

Knowledge of $M(T, H, p)$ enables us to compute the isothermal entropy changes associated with the caloric and multicaloric effects of $\text{Fe}_{49}\text{Rh}_{51}$, as described in Sec. III. Entropy changes determined for standard magnetocaloric [$\Delta S(T, 0 \rightarrow H, p = 0)$] and standard barocaloric [$\Delta S(T, H = 0, 0 \rightarrow p)$] effects are in excellent agreement with those previously obtained by quasidirect and direct calorimetric measurements [26]. This good agreement provides high confidence in the computation of entropy changes at arbitrary values of pressure and magnetic field that quantify the multicaloric response of the material.

In computing multicaloric effects in $\text{Fe}_{49}\text{Rh}_{51}$ from experimental data, attention must be paid to the fact that application of magnetic field stabilizes the FM phase, whereas application of pressure stabilizes the AFM phase. Also, the noted hysteresis of the transition implies that simultaneous (or subsequent) application of both magnetic field and pressure will take the sample through a minor loop within the two-phase coexistence region (i.e., the region bounded by the two planes in Fig. 5, and between two magnetization surfaces in Fig. 4). As detailed trajectories of these minor loops are not accessible from present experimental data, study of the $\text{Fe}_{49}\text{Rh}_{51}$ multicaloric response will be restricted to experimental values obtained from application of the magnetic field and the removal of hydrostatic pressure (i.e., trajectories on the AFM to FM surface, see Fig. 4). In the phase diagram of Fig. 5, they correspond to trajectories from below the red plane to above the red plane. An equivalent analysis could be done for the application of pressure and removal of magnetic field (FM to AFM transition, trajectories from above the blue plane to below the blue plane, Fig. 5), but for the sake of conciseness this case will not be considered here.

The multicaloric isothermal entropy change has been computed from experimental data according to Eq. (3) where the limits for the integrals in pressure are computed from an arbitrary p value to zero.

Examples for the multicaloric entropy change computed at two selected values of temperature are plotted in Fig. 7 as colored contour maps. The plotted values correspond to the (simultaneous or sequential) application of a magnetic field from a value of zero to a given magnetic field, indicated by the vertical scale, and to the removal of hydrostatic pressure from a value of 5 kbar down to an arbitrary pressure given by the horizontal scale (pressure drop), i.e., $\Delta S(T, 0 \rightarrow H, 5 \text{ kbar} \rightarrow p)$. It is seen that ΔS increases with increasing magnetic field and increasing pressure drop, up to a saturation value around $11 \text{ J kg}^{-1} \text{ K}^{-1}$ which coincides with the reported transition entropy change for the magnetostructural transition in $\text{Fe}_{49}\text{Rh}_{51}$. It is noted that the material exhibits a large entropy change over a broad range of magnetic field and pressure

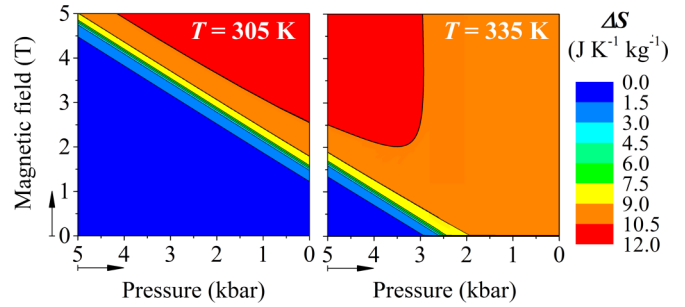


FIG. 7. Colored contour maps of the multicaloric entropy change of the $\text{Fe}_{49}\text{Rh}_{51}$ corresponding to the application of a magnetic field H ($0 \rightarrow H$) and to the removal of a pressure p from an initial pressure of 5 kbar ($5 \text{ kbar} \rightarrow p$).

values. Importantly, the larger the pressure drop, the smaller the magnetic field required to achieve the saturation value; conversely, the larger the magnetic field applied, the smaller the pressure drop required. It is also remarkable that the region where ΔS increases from zero to the maximum value (the multicolored band in Fig. 7) is rather narrow, indicative of a very large multicaloric strength. The small decrease in ΔS observed at $T = 335 \text{ K}$ for large values of pressure drop is a consequence of the previously mentioned small decrease in the transition magnetization change (ΔM_t). Indeed, application of magnetic field slightly increases the values for the pressure induced entropy change.

We have computed the temperature dependence of the multicaloric entropy change corresponding to the application of a 2 T magnetic field and a pressure drop from 5 kbar to 0. Results are shown in Fig. 8(a), with solid lines corresponding

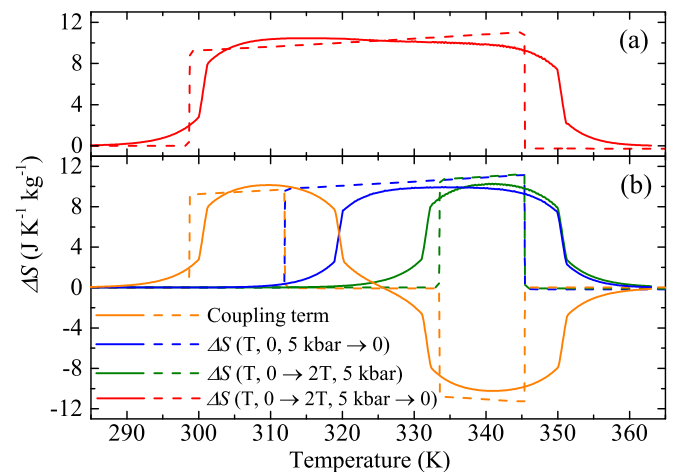


FIG. 8. (a) Temperature dependence of the multicaloric entropy change in $\text{Fe}_{49}\text{Rh}_{51}$ corresponding to the isothermal application of a 2 T magnetic field and the removal of 5 kbar pressure. (b) Temperature dependence of the isothermal entropy change corresponding to the magnetocaloric effect (green lines), to the barocaloric effect (blue lines), and to the interplay between magnetism and structure (orange line). In all panels, solid lines correspond to values computed from experiments and dashed lines correspond to values computed from the mean field model.

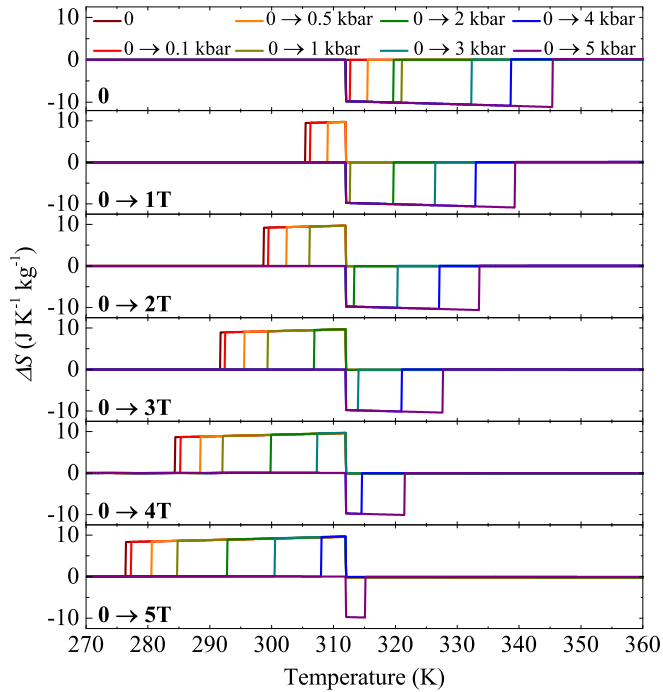


FIG. 9. Temperature dependence of the multicaloric isothermal entropy change, $\Delta S(T, 0 \rightarrow H, 0 \rightarrow p)$ for selected values of applied magnetic field and applied hydrostatic pressure.

to experimental data and dashed lines to the data obtained from the mean field model. Good coincidence is noted between the two sets of data except for a tiny region at high temperatures. In Fig. 8(b) we have emphasized the different contributions to the multicaloric entropy change where the green curve indicates the entropy change resulting from the application of a 2 T magnetic field under a pressure of 5 kbar [$\Delta S(T, 0 \rightarrow 2T, 5 \text{ kbar})$] and the blue curve indicates the entropy change resulting from the removal of a 5 kbar pressure in the absence of magnetic field [$\Delta S(T, 0, 5 \text{ kbar} \rightarrow 0)$]. The value for the cross-response contribution [last term in Eq. (3)] is plotted in orange lines.

From Fig. 8 it is seen that a suitable combination of magnetic field and pressure significantly expands the temperature range where large (giant) values of the entropy change are obtained. It is apparent that magnetocaloric and barocaloric effects are restricted to a narrow temperature window, and the large ΔS values obtained at the low temperature region arise from the cross-response coupling between magnetic and structural degrees of freedom. It is worth noting that a large temperature window for the entropy change not only results in a larger operational range in potential refrigeration devices, but also increases the reproducibility of these large entropy values upon pressure and magnetic field cycling.

Taking into account that results derived from the mean field model do not include hysteresis, we can gain insight on the multicaloric behavior obtained upon application (or removal) of the two fields by computing $\Delta S(T, 0 \rightarrow H, 0 \rightarrow p)$ from the model. In Fig. 9 the temperature dependence of the multicaloric isothermal entropy change $\Delta S(T, 0 \rightarrow H, 0 \rightarrow p)$ is plotted for selected values of the applied magnetic field and

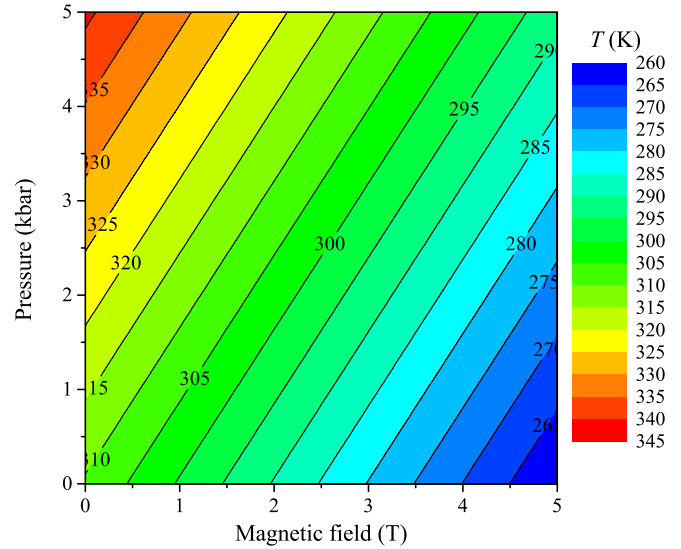


FIG. 10. Isothermal contour lines where multicaloric entropy reverses its sign.

hydrostatic pressure, obtained as

$$\Delta S(T, 0 \rightarrow H, 0 \rightarrow p) = S(T, H, p) - S(T, H = 0, p = 0). \quad (14)$$

The inverse nature of the magnetocaloric effect combined with the conventional barocaloric effect results in a peculiar multicaloric response in Fe₄₉Rh₅₁. At low values of magnetic field (top panels in Fig. 9), the barocaloric effect dominates and application of pressure reduces the total entropy. As the magnetic field magnitude is increased, the inverse effect gains significance as evident by the expanded temperature window where the entropy change is positive. Interestingly, the multicaloric ΔS reverses sign for particular combinations of pressure and magnetic field. This effect is described in more detail in Fig. 10 which depicts the isothermal lines on a (H, p) plane where the multicaloric ΔS reverses its sign. These lines are projections of the phase diagram [see Fig. 5(a)] onto the (H, p) (horizontal) plane. For H and p values to the right of each isothermal line, the multicaloric entropy change $\Delta S(T, 0 \rightarrow H, 0 \rightarrow p) > 0$, while for values on the left-hand side, $\Delta S(T, 0 \rightarrow H, 0 \rightarrow p) < 0$. It is therefore demonstrated that very fine tuning of the caloric and multicaloric response can be achieved by simultaneous (or sequential) application of magnetic field and pressure to this FeRh system.

IX. SUMMARY AND CONCLUSIONS

To summarize, we have presented a comprehensive study of the multicaloric behavior of Fe₄₉Rh₅₁ where the mechanical and magnetic contributions have been determined, as well as the contributions due to the cross response of the alloy arising from the interplay between magnetism and structure. The present work also exhibits how a mean field model can be useful in computing the multicaloric effect in a complex system such as Fe₄₉Rh₅₁. In Fe₄₉Rh₅₁ application of a magnetic field results in just a small increase of the pressure-induced entropy change because the magnetostructural transition occurs well below the Curie point, but for materials with a

magnetostructural transition close to the Curie point it is expected that the combined effect of pressure and magnetic field can result in a significant enhancement of the entropy change corresponding to standard barocaloric and magnetocaloric effects. It has been shown that the combined effect of two external stimuli leads to interesting multicaloric properties: it is possible to enlarge the temperature window where giant effects are observed, and also, the caloric response can be turned from conventional to inverse by proper combinations of pressure and magnetic field. In particular, when p and H are close to the values that reverse the sign of the multicaloric entropy change, a fine tuning of one of these two parameters results in a completely different caloric response of the material that can shift the material from heating to cooling. This switching in the multicaloric response opens up a new field of potential applications in which devices can be brought from heating to cooling by suitable small changes in the control parameters.

ACKNOWLEDGMENTS

We acknowledge financial support from the Spanish Ministry of Science (MAT2016-75823-R) and from Northeastern University. E.S.-T. acknowledges support from AGAUR (Catalonia).

APPENDIX A: THERMODYNAMICS OF MULTICALORIC EFFECTS

In this Appendix we summarize the thermodynamics of multicaloric effects [10] in the particular case systems with baromagnetic coupling. The fundamental thermodynamic identity is given in this case by

$$dU = TdS - pdV + HdM, \quad (\text{A1})$$

and the generalized Helmholtz and Gibbs potentials are given respectively by

$$\begin{aligned} d\mathcal{F} &= -SdT - pdV + HdM, \\ d\mathcal{G} &= -SdT + Vdp - MdH, \end{aligned} \quad (\text{A2})$$

rendering the following Maxwell relations

$$\left(\frac{\partial S}{\partial V}\right)_{T,M} = \left(\frac{\partial p}{\partial T}\right)_{V,M}, \quad (\text{A3})$$

$$\left(\frac{\partial S}{\partial M}\right)_{T,M} = -\left(\frac{\partial H}{\partial T}\right)_{V,M}, \quad (\text{A4})$$

$$\left(\frac{\partial S}{\partial p}\right)_{T,M} = -\left(\frac{\partial V}{\partial T}\right)_{p,H}, \quad (\text{A5})$$

$$\left(\frac{\partial S}{\partial H}\right)_{T,p} = \left(\frac{\partial M}{\partial T}\right)_{p,H}, \quad (\text{A6})$$

$$\left(\frac{\partial V}{\partial H}\right)_{T,p} = -\left(\frac{\partial M}{\partial p}\right)_{T,H}. \quad (\text{A7})$$

Notice that the last Maxwell relation (A7) establishes that the two cross susceptibilities are equal.

The change of entropy induced by an applied magnetic field at zero pressure that quantifies the standard magnetocaloric

effect is given by

$$\begin{aligned} \Delta S_{\text{MCE}} &= \Delta S(T, 0 \rightarrow H, p = 0) \\ &= \int_0^H \left(\frac{\partial S}{\partial H}\right)_{T,p} dH = \int_0^H \left(\frac{\partial M}{\partial T}\right)_{p,H} dH, \end{aligned} \quad (\text{A8})$$

where we have assumed $S = S(T, p, H)$ and we have used the Maxwell relation (A6). Similarly, the standard barocaloric effect is given by

$$\begin{aligned} \Delta S_{\text{BCE}} &= \Delta S(T, H = 0, 0 \rightarrow p) \\ &= \int_0^p \left(\frac{\partial S}{\partial p}\right)_{T,H} dp = -\int_0^p \left(\frac{\partial V}{\partial T}\right)_{p,H} dp, \end{aligned} \quad (\text{A9})$$

where we have used the appropriate Maxwell relation (A5). In the case of combined application of both external fields, the multicaloric effect is given by

$$\begin{aligned} \Delta S(T, 0 \rightarrow H, 0 \rightarrow p) &= \Delta S(T, H = 0, 0 \rightarrow p) + \Delta S(T, 0 \rightarrow H, p) \\ &= \Delta S_{\text{BCE}} + \Delta S_{\text{MCE}} \\ &\quad + \int_0^p \frac{\partial}{\partial p'} [\Delta S(T, 0 \rightarrow H, p')]_{T,H} dp'. \end{aligned} \quad (\text{A10})$$

The last term in the above expression, which accounts for the interplay between magnetism and volume, can be expressed as

$$\begin{aligned} &\int_0^p \frac{\partial}{\partial p'} [\Delta S(T, 0 \rightarrow H, p')]_{T,H} dp' \\ &= \int_0^p \frac{\partial}{\partial p'} \left[\int_0^H \left(\frac{\partial M}{\partial T}\right)_{H,p'} dH \right]_{T,H} dp' \\ &= \int_0^p \int_0^H \frac{\partial}{\partial T} \left(\frac{\partial M}{\partial p}\right)_{T,H} dp dH. \end{aligned} \quad (\text{A11})$$

Given the relation (A7) it is possible to see that

$$\begin{aligned} &\int_0^p \frac{\partial}{\partial p'} [\Delta S(T, 0 \rightarrow H, p')]_{T,H} dp' \\ &= \int_0^H \frac{\partial}{\partial H'} [\Delta S(T, H', 0 \rightarrow p)]_{T,p} dH', \end{aligned} \quad (\text{A12})$$

consistently with the fact that, from a thermodynamic point of view, there is no distinction on whether both fields are applied simultaneously or sequentially.

In some cases, it can be convenient to consider the entropy as a function of the extensive variables instead of the conjugated fields. That is, we now assume that $S = S(T, M, V)$. In that case, the standard barocaloric effect can be expressed as

$$\begin{aligned} \Delta S_{\text{BCE}} &= \int_{M(p=0)}^{M(p)} \left(\frac{\partial S}{\partial M}\right)_{T,V} dM \\ &= -\int_{M(p=0)}^{M(p)} \left(\frac{\partial H}{\partial T}\right)_{V,M} dM, \end{aligned} \quad (\text{A13})$$

where we have assumed that magnetization effects are dominant and we have used the relation (A4). The differential inside

the integral can be expressed as

$$dM = \left(\frac{\partial M}{\partial p} \right)_{T, H=0} dp \quad (\text{A14})$$

and

$$\left(\frac{\partial H}{\partial T} \right)_M = - \left(\frac{\partial M}{\partial T} \right)_H \left(\frac{\partial H}{\partial M} \right)_T. \quad (\text{A15})$$

Introducing (A14) and (A15) into (A13) we obtain the following expression for the barocaloric effect:

$$\Delta S_{\text{BCE}} \simeq \int_0^p \frac{\left(\frac{\partial M}{\partial p} \right)_{T, H}}{\left(\frac{\partial M}{\partial H} \right)_{T, p}} \left(\frac{\partial M}{\partial T} \right)_{p, H} dp. \quad (\text{A16})$$

APPENDIX B: THE MEAN FIELD MODEL

We start by dividing the CsCl structure of the equiatomic FeRh alloy into four sublattices, two (labeled α and γ) occupied by Fe atoms and two (labeled β and δ) occupied by Rh atoms. Next, we define the following magnetic order parameters in terms of the sublattice magnetizations:

$$m_{\text{Fe}} = \frac{m_\alpha + m_\gamma}{2}, \quad m_{\text{Rh}} = \frac{m_\beta + m_\delta}{2}, \quad (\text{B1})$$

and

$$\eta_{\text{Fe}} = \frac{m_\alpha - m_\gamma}{2}. \quad (\text{B2})$$

Where m_{Fe} and m_{Rh} represent the ferromagnetic order parameters of Fe and Rh, respectively, while η_{Fe} is the antiferromagnetic order parameter of Fe. Thus, the total magnetization is given by $M = m_{\text{Fe}} + m_{\text{Rh}}$.

The energy of the system in terms of the occupation probabilities $\{\pi\}$ for the different sublattices can be written as

$$\begin{aligned} \langle H \rangle &= Nz J_{\text{Fe-Rh}}^{(1)} \sum_{\mu=\alpha, \gamma; \nu=\beta, \delta} (\pi_\mu^+ \pi_\nu^- + \pi_\mu^- \pi_\nu^+) \\ &+ \frac{Ny}{2} J_{\text{Fe-Fe}}^{(2)} (\pi_\alpha^+ \pi_\gamma^- + \pi_\alpha^- \pi_\gamma^+) \\ &+ \frac{Ny}{2} J_{\text{Rh-Rh}}^{(2)} (\pi_\beta^+ \pi_\delta^- + \pi_\beta^- \pi_\delta^+) + E_0, \end{aligned} \quad (\text{B3})$$

with the constant E_0 given by

$$E_0 = -N \left(\frac{z}{2} J_{\text{Fe-Rh}}^{(1)} + \frac{y}{4} J_{\text{Fe-Fe}}^{(2)} + \frac{y}{4} J_{\text{Rh-Rh}}^{(2)} \right). \quad (\text{B4})$$

Superscripts (1) and (2) in the effective interaction parameters (J) denote first and second neighbor pairs, respectively, N is the number of magnetic atoms, and z and y are the coordination numbers for first and second neighbors, respectively. The variables π_σ^+ and π_σ^- represent the probabilities that a σ site ($\sigma = \alpha, \beta, \gamma, \delta$) be occupied by an atom with magnetic moment up (+) and down (-), respectively. Moreover, the occupation probabilities π_σ^+ and π_σ^- depend on the sublattice magnetization m_σ . That is,

$$\pi_\sigma^\pm = \frac{(1 \pm m_\sigma)}{2}. \quad (\text{B5})$$

Introducing (B5) into (B3), and using the definitions in Eqs. (B1) and (B2), we obtain the following expression for the

energy of the magnetic alloy in terms of the order parameters of the two components:

$$\begin{aligned} \langle H \rangle &= - \frac{Nz}{2} J_{\text{Fe-Rh}}^{(1)} m_{\text{Fe}} m_{\text{Rh}} \\ &- \frac{Ny}{4} J_{\text{Fe-Fe}}^{(2)} (m_{\text{Fe}}^2 - \eta_{\text{Fe}}^2) - \frac{Ny}{4} J_{\text{Rh-Rh}}^{(2)} m_{\text{Rh}}^2, \end{aligned} \quad (\text{B6})$$

where $J_{\text{Fe-Rh}}^{(1)}$ is taken to be positive. To obtain the free energy, we need the expression of the model entropy that in terms of the occupation probabilities can be written as

$$S = - \frac{Nk_B}{2} \sum_{\sigma=\alpha, \beta, \gamma, \delta} (\pi_\sigma^+ \ln \pi_\sigma^+ + \pi_\sigma^- \ln \pi_\sigma^-). \quad (\text{B7})$$

Finally, the magnetic free energy per magnetic atom can be written as

$$\begin{aligned} f_{\text{mag}}(T, m_{\text{Fe}}, m_{\text{Rh}}, \eta_{\text{Fe}}) &= \frac{\langle H \rangle}{N} - T \frac{S}{N} = - \frac{z}{2} J_{\text{Fe-Rh}}^{(1)} m_{\text{Fe}} m_{\text{Rh}} \\ &- \frac{y}{4} J_{\text{Fe-Fe}}^{(2)} (m_{\text{Fe}}^2 - \eta_{\text{Fe}}^2) - \frac{y}{4} J_{\text{Rh-Rh}}^{(2)} m_{\text{Rh}}^2 \\ &+ \frac{k_B T}{8} [(1 + m_{\text{Fe}} + \eta_{\text{Fe}}) \ln(1 + m_{\text{Fe}} + \eta_{\text{Fe}}) \\ &+ (1 - m_{\text{Fe}} - \eta_{\text{Fe}}) \ln(1 - m_{\text{Fe}} - \eta_{\text{Fe}}) \\ &+ (1 + m_{\text{Fe}} - \eta_{\text{Fe}}) \ln(1 + m_{\text{Fe}} - \eta_{\text{Fe}}) \\ &+ (1 - m_{\text{Fe}} + \eta_{\text{Fe}}) \ln(1 - m_{\text{Fe}} + \eta_{\text{Fe}}) \\ &+ 2(1 + m_{\text{Rh}}) \ln(1 + m_{\text{Rh}}) \\ &+ 2(1 - m_{\text{Rh}}) \ln(1 - m_{\text{Rh}}) - 8 \ln 2], \end{aligned} \quad (\text{B8})$$

where, consistently with the fact that Rh does not exhibit antiferromagnetic order, we have required that sublattices β and δ to be equivalent, that is $m_\beta = m_\delta$. A characteristic of FeRh alloys is that its unit cell volume changes at the magnetostructural transition. To account for this feature, we incorporate the following (magnetovolumic) coupling terms between the magnetic order parameters and the volume change w (relative to a reference volume Ω_0), restricted to the minimum order allowed by symmetry:

$$f_{\text{coupling}} = \frac{1}{2} \alpha_0 w^2 - \alpha_1 w (m_{\text{Fe}} + m_{\text{Rh}})^2 - \alpha_2 w \eta_{\text{Fe}}^2, \quad (\text{B9})$$

with α_1 and α_2 as magnetostriction coefficients and α_0 as the inverse of the compressibility. Indeed, expression (B9) preserves the reverse sign fundamental symmetry of the magnetic order parameters present in Eq. (B8). Therefore, the lowest-order term for (isotropic) magnetovolumic coupling has to be linear in the volume and quadratic in the magnetic order parameters. We now proceed by simply appending the coupling term (B9) to the expression (B8) so that the total free energy of the system is $f = f_{\text{mag}} + f_{\text{coupling}}$. Furthermore, it is convenient to include the effect of external magnetic and hydrostatic fields which yields the following expression for the total Gibbs free energy of the system in reduced units:

$$\begin{aligned} g^* &= \frac{g}{z J_{\text{Fe-Rh}}^{(1)}} = - \frac{1}{2} m_{\text{Fe}} m_{\text{Rh}} - \frac{J^*}{4} (m_{\text{Fe}}^2 - \eta_{\text{Fe}}^2) \\ &+ \frac{T^*}{8} [(1 + m_{\text{Fe}} + \eta_{\text{Fe}}) \ln(1 + m_{\text{Fe}} + \eta_{\text{Fe}}) \\ &+ (1 - m_{\text{Fe}} - \eta_{\text{Fe}}) \ln(1 - m_{\text{Fe}} - \eta_{\text{Fe}}) \\ &+ (1 + m_{\text{Fe}} - \eta_{\text{Fe}}) \ln(1 + m_{\text{Fe}} - \eta_{\text{Fe}}) \\ &+ (1 - m_{\text{Fe}} + \eta_{\text{Fe}}) \ln(1 - m_{\text{Fe}} + \eta_{\text{Fe}}) \\ &+ 2(1 + m_{\text{Rh}}) \ln(1 + m_{\text{Rh}}) \\ &+ 2(1 - m_{\text{Rh}}) \ln(1 - m_{\text{Rh}}) - 8 \ln 2], \end{aligned}$$

$$\begin{aligned}
& + (1 - m_{\text{Fe}} - \eta_{\text{Fe}}) \ln(1 - m_{\text{Fe}} - \eta_{\text{Fe}}) \\
& + (1 + m_{\text{Fe}} - \eta_{\text{Fe}}) \ln(1 + m_{\text{Fe}} - \eta_{\text{Fe}}) \\
& + (1 - m_{\text{Fe}} + \eta_{\text{Fe}}) \ln(1 - m_{\text{Fe}} + \eta_{\text{Fe}}) \\
& + 2(1 + m_{\text{Rh}}) \ln(1 + m_{\text{Rh}}) + 2(1 - m_{\text{Rh}}) \ln(1 - m_{\text{Rh}}) \\
& - 8 \ln 2] + \frac{1}{2} \alpha_0^* w^2 - \alpha_1^* w (m_{\text{Fe}} + m_{\text{Rh}})^2 - \alpha_2^* w \eta_{\text{Fe}}^2 \\
& - H^*(m_{\text{Fe}} + m_{\text{Rh}}) + P \Omega_0^* w, \tag{B10}
\end{aligned}$$

where for the sake of simplicity we have set $J_{\text{Rh-Rh}} = 0$ and the superscript (*) indicates that the corresponding term magnitude is given in units of ($zJ_{\text{Fe-Rh}}^{(1)}$). We stress that the previous equation corresponds to a variational function. The thermodynamic free energy which is a Legendre transform of the internal energy is a function of $g^*(T, p, H)$ and corresponds to substitute the order parameters for those that, at a given T , minimize the function (B10). The entropy can then be computed directly by taking into account that

$$\begin{aligned}
S(M_{\text{Fe}}, m_{\text{Rh}}, \eta_{\text{Fe}}) \\
= - \left[\frac{\partial g^*}{\partial T^*} \right]_{P, H} = \frac{1}{8} [(1 + m_{\text{Fe}} + \eta_{\text{Fe}}) \ln(1 + m_{\text{Fe}} + \eta_{\text{Fe}})
\end{aligned}$$

$$\begin{aligned}
& + (1 - m_{\text{Fe}} - \eta_{\text{Fe}}) \ln(1 - m_{\text{Fe}} - \eta_{\text{Fe}}) \\
& + (1 + m_{\text{Fe}} - \eta_{\text{Fe}}) \ln(1 + m_{\text{Fe}} - \eta_{\text{Fe}}) \\
& + (1 - m_{\text{Fe}} + \eta_{\text{Fe}}) \ln(1 - m_{\text{Fe}} + \eta_{\text{Fe}}) \\
& + 2(1 + m_{\text{Rh}}) \ln(1 + m_{\text{Rh}}) \\
& + 2(1 - m_{\text{Rh}}) \ln(1 - m_{\text{Rh}}) - 8 \ln 2] \\
& = S_{\text{Fe}}(m_{\text{Fe}}, \eta_{\text{Fe}}) + S_{\text{Rh}}(m_{\text{Rh}}). \tag{B11}
\end{aligned}$$

In the present work, the expression for the total Gibbs free energy of the model (B10) has been solved for $\alpha_1^* = 0.30$, $\alpha_2^* = -0.4241$, and $J^* = -0.96$. It is worth mentioning that the equilibrium magnetic order configurations have been obtained by requiring the Rh magnetic moment in the AFM phase to be $\mu_{\text{Rh}} = 0$. Accordingly, we have considered that the number of magnetic atoms in the FM phase is twice that of the AFM phase. Moreover, the model has been fitted to experimental data for the transition temperatures of equiatomic and nearly equiatomic FeRh both at atmospheric pressure and at the applied pressure where the FM disappears [26,30–32], and to the relative volume change at the FM-AFM magnetostructural transition. The obtained estimates for the effective exchange constant $J_{\text{Fe-Rh}}^{(1)} = 10.2$ meV and for the unit cell volume $\Omega_0 = 17.9 \times 10^{-30}$ m³ are in good agreement with previously reported values [35–37].

-
- [1] S. Fähler *et al.*, *Adv. Eng. Mater.* **14**, 10 (2012).
[2] L. Mañosa, A. Planes, and M. Acet, *J. Mater. Chem. A* **1**, 4925 (2013).
[3] X. Moya, S. Kar-Narayan, and N. D. Mathur, *Nat. Mater.* **13**, 439 (2014).
[4] K. A. Gschneidner, V. K. Pecharsky, and A. O. Tsokol, *Rep. Prog. Phys.* **68**, 1479 (2005).
[5] M. Valant, *Prog. Mater. Sci.* **57**, 980 (2012).
[6] L. Mañosa and A. Planes, *Adv. Mater.* **29**, 1603607 (2017).
[7] X. Moya and N. D. Mathur, *APL Mater.* **4**, 063701 (2016).
[8] M. Vopson, *Solid State Commun.* **152**, 2067 (2012).
[9] S. Lisenkov, B. K. Mani, C.-M. Chang, J. Almand, and I. Ponomareva, *Phys. Rev. B* **87**, 224101 (2013).
[10] A. Planes, T. Castán, and A. Saxena, *Philos. Mag.* **94**, 1893 (2014).
[11] A. Planes, T. Castán, and A. Saxena, *Philos. Trans. R. Soc. London Sect. A* **374**, 20150304 (2016).
[12] S. Gama, A. A. Coelho, A. deCampos, A.M. Carvalho, F. C. G. Gandra, P. J. von Ranke, and N. A. de Oliveira, *Phys. Rev. Lett.* **93**, 237202 (2004).
[13] J. Lyubina, K. Nenkov, L. Schultz, and O. Gutfleisch, *Phys. Rev. Lett.* **101**, 177203 (2008).
[14] P. O. Castillo-Villa *et al.*, *Phys. Rev. B* **83**, 174109 (2011).
[15] T. Samanta, D. L. Lepkowski, A. U. Saleheen, A. Shankar, J. Prestigiacomo, I. Dubenko, A. Quetz, I. W. H. Oswald, G. T. McCandless, J. Y. Chan, P. W. Adams, D. P. Young, N. Ali, and S. Stadler, *Phys. Rev. B* **91**, 020401(R) (2015).
[16] J. Liu, T. Gottschall, K. P. Skokov, J. D. Moore, and O. Gutfleisch, *Nat. Mater.* **11**, 620 (2012).
[17] R. Barua, I. McDonald, F. Jiménez-Villacorta, D. Heiman, and L. H. Lewis, *J. Alloys Compd.* **689**, 1044 (2016).
[18] L. H. Lewis, C. H. Marrows, and S. Langridge, *J. Phys. D: Appl. Phys.* **49**, 323002 (2016).
[19] R. Witte, R. Kruk, M. E. Gruner, R. A. Brand, D. Wang, S. Schlabach, A. Beck, V. Provenzano, R. Pentcheva, H. Wende, and H. Hahn, *Phys. Rev. B* **93**, 104416 (2016).
[20] S. O. Mariager, F. Pressacco, G. Ingold, A. Caviezel, E. Mohr-Vorobeva, P. Beaud, S. L. Johnson, C. J. Milne, E. Mancini, S. Moyerman, E. E. Fullerton, R. Feidenhansl, C. H. Back, and C. Quitmann, *Phys. Rev. Lett.* **108**, 087201 (2012).
[21] D. W. Cooke, F. Hellman, C. Baldasseroni, C. Bordel, S. Moyerman, and E. E. Fullerton, *Phys. Rev. Lett.* **109**, 255901 (2012).
[22] Y. Liu, L. C. Phillips, R. Mattana, M. Bibes, A. Barthélémy, and B. Dhillon, *Nat. Commun.* **7**, 11614 (2016).
[23] G. Shirane, R. Nathans, and C. W. Chen, *Phys. Rev. B* **134**, A1547 (1964).
[24] S. Nikitin, G. Myalikgulyev, A. M. Tishin, M. P. Annaorazov, K. A. Asatryan, and A. L. Tyurin, *Phys. Lett. A* **148**, 363 (1990).
[25] S. Nikitin, G. Myalikgulyev, M. P. Annaorazov, A. L. Tyurin, R. W. Myndev, and S. A. Akopyan, *Phys. Lett. A* **171**, 234 (1992).
[26] E. Stern-Taulats, A. Planes, P. Lloveras, M. Barrio, J. L. Tamarit, S. Pramanick, S. Majumdar, C. Frontera, and L. Manosa, *Phys. Rev. B* **89**, 214105 (2014).
[27] E. Stern-Taulats *et al.*, *Appl. Phys. Lett.* **107**, 152409 (2015).

- [28] A. Chirkova, K. P. Skokov, L. Schultz, N. V. Baranov, O. Gutfleisch, and T. G. Woodcock, *Acta Mater.* **106**, 15 (2016).
- [29] G. T. Dubovka, *Zh. Eksp. Teor. Fiz.* **65**, 2282 (1973) [*J. Exper. Theor. Phys.* **38**, 1140 (1974)].
- [30] E. G. Ponyatovskii, A. R. Kutsar, and G. T. Dubovka, *Kristallografiya* **12**, 79 (1967) [*Sov. Phys.-Crystallogr.* **12**, 63 (1967)].
- [31] A. I. Zakharov, A. M. Kadomtseva, R. Z. Levitin, and E. G. Ponyatovskii, *Zh. Eksp. Teor. Fiz.* **46**, 2003 (1964) [*J. Exper. Theor. Phys.* **19**, 1348 (1964)].
- [32] L. I. Vinokurova, A. V. Vlasov, and M. Pardavi-Horvath, *Phys. Status Solidi B* **78**, 353 (1976).
- [33] E. Stern-Taulats, P. O. Castillo-Villa, L. Mañosa, C. Frontera, S. Pramanick, S. Majumdar, and A. Planes, *J. Appl. Phys.* **115**, 173907 (2014).
- [34] O. Gutfleisch, T. Gottschall, M. Fries, D. Benke, I. Radulov, K. P. Skokov, H. Wende, M. Gruner, M. Acet, P. Entel, and M. Farle, *Philos. Trans. R. Soc. London Sect. A* **374**, 20150308 (2016).
- [35] R. Barua, F. Jiménez-Villacorta, and L. H. Lewis, *Appl. Phys. Lett.* **103**, 102407 (2013).
- [36] J. Kudrnovsky, V. Drchal, and I. Turek, *Phys. Rev. B* **91**, 014435 (2015).
- [37] R. Y. Gu and V. P. Antropov, *Phys. Rev. B* **72**, 012403 (2005).